



6

Frequency-domain Characterization of Signals and Systems

Many biomedical systems exhibit innate rhythms and periodicity: more readily expressed and appreciated in terms of frequency than time units.



Cardiac rhythm more conveniently expressed in

beats per minute,

a measure of frequency of occurrence or rate of repetition,

than in terms of duration of a beat or

interval between beats in seconds (*RR* interval).

Cardiac rhythm expressed as *72 bpm* more easily

understood than the corresponding *RR* interval as *0.833 s*.



EEG rhythm conveyed more readily by description in

cycles per second or in *Hertz (Hz)*

than a time-domain description:

alpha rhythm having a frequency of 11.5 Hz

versus the equivalent period of 0.087 s .



PCG: interesting example of a signal with multiple frequency-domain features.

Beat-to-beat periodicity or rhythm.

Heart sounds within a cardiac cycle exhibit *resonance*.

Multi-compartmental nature of the cardiac system:

multiple resonance frequencies: composite *spectrum* of several dominant or resonance frequencies.



Constrained flow of blood through an orifice (septal defect)

or across a stenosed valve acting as a baffle

leads to turbulence: *wide-band noise*.

Need to consider the distribution of the signal's energy or

power over a wide band of frequencies:

leads to the notion of the power *spectral density* function.



6.1 Problem Statement

Investigate the potential use of the Fourier spectrum and parameters thereof in the analysis of biomedical signals.

Identify physiological and pathological processes that could modify the frequency content of the corresponding signals.

Outline the signal processing tasks needed to perform spectral analysis of biomedical signals and systems.



6.2 Illustration of the Problem with Case-studies

6.2.1 *The effect of myocardial elasticity on heart sound spectra*

The first and second heart sounds — S1 and S2 — are typically composed of low-frequency components, due to the fluid-filled and elastic nature of the cardiovascular system.



Sakai et al. processed recorded heart sound signals by using tunable bandpass filters, with a bandwidth of 20 Hz , tuned over the range $20 - 40\text{ Hz}$ to $400 - 420\text{ Hz}$, and estimated the frequency distributions of S1 and S2.

Heart sound spectra maximum in the $20 - 40\text{ Hz}$ band;

S1: peaks at lower frequencies than those of S2;

S2: “gentle peaking” between 60 Hz and 220 Hz .



Gerbarg et al.: computer program to simulate a filter bank.

Obtained averaged power spectra of S1 and S2 of

1,000 adult males,

32 high-school children, and 75 patients in a hospital.

Averaged PSDs of S1 and S2:

peak power in the range $60 - 70 \text{ Hz}$,

power levels lower than -10 dB beyond 150 Hz .

PSD of S2: more high-frequency energy than S1.



Yoganathan et al.: FFT analysis of S1 and S2.

Spectra of 250 ms windows with S1 averaged over 15 beats.

Spectrum of S1:

peaks in a low-frequency range ($10 - 50\text{ Hz}$)

and a medium-frequency range ($50 - 140\text{ Hz}$).



Spectrum of S2: peaks in low-frequency ($10 - 80 \text{ Hz}$),

medium-frequency ($80 - 220 \text{ Hz}$),

and high-frequency ranges ($220 - 400 \text{ Hz}$).

Spectral peaks related to resonance and the

elastic properties of heart muscles.



Adolph et al.: dynamic spectrum analyzer to study

frequency content of S1 during iso-volumic contraction.

Center frequency of filter with 20 Hz bandwidth

varied from 30 Hz to 70 Hz , in steps of 10 Hz .

Outputs of filters averaged over 10 consecutive beats.

Ratios of the average peak voltage of the filtered outputs

to that of full S1 during iso-volumic contraction computed.



Adolph et al. hypothesized that frequency content of S1 during iso-volumic contraction should depend on relative contributions of mass and elasticity of left ventricle.

Mass of left ventricle with blood content remains constant during iso-volumic contraction.

Frequency content of S1 decreases in case of diseases that reduce ventricular elasticity: myocardial infarction.

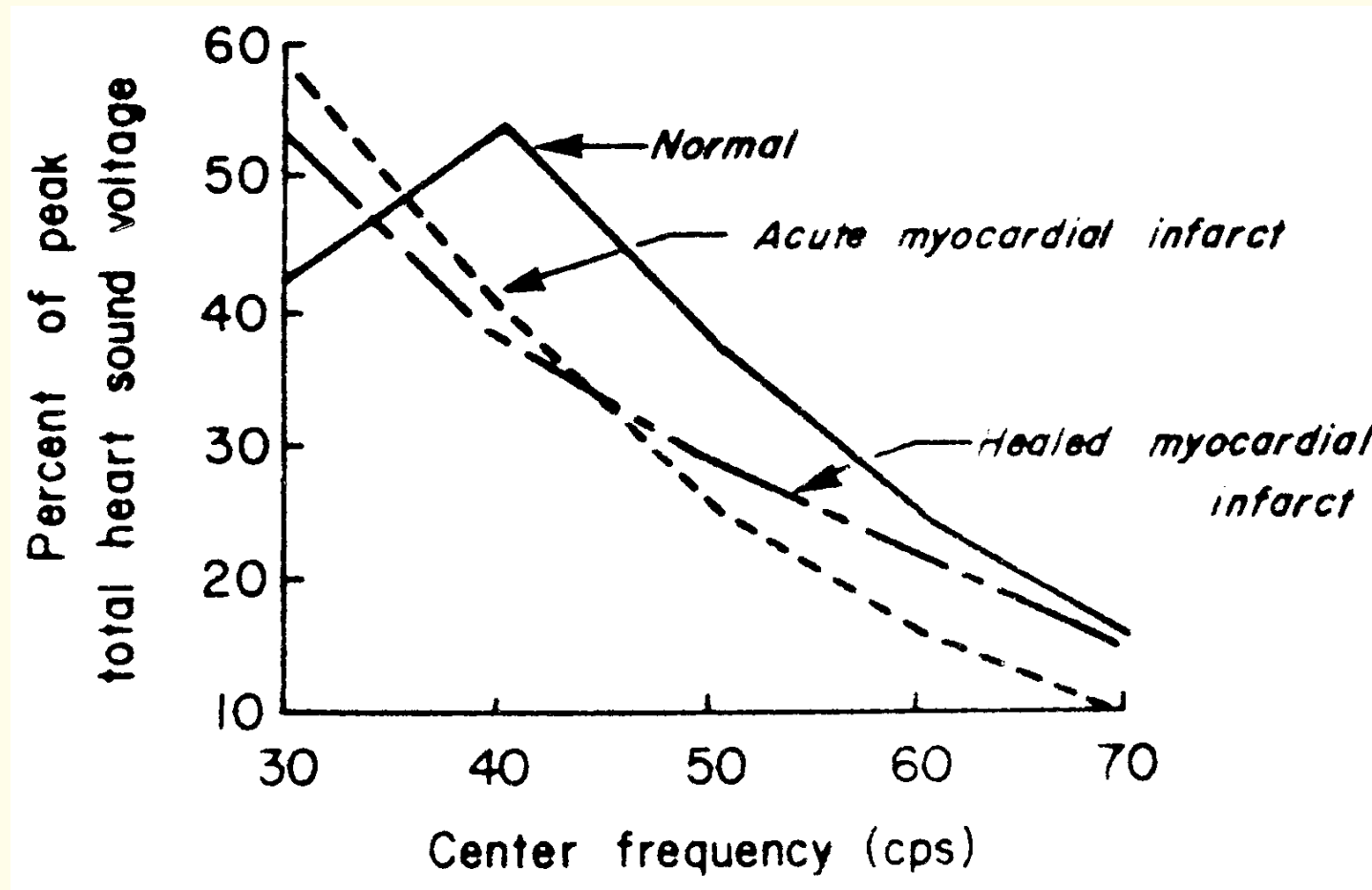


Figure 6.1: First heart sound spectra for normal, acute myocardial infarct, and healed myocardial infarct cases. The latter two cases exhibit an increased percentage of low-frequency components. Reproduced with permission from R.J. Adolph, J.F. Stephens, and K. Tanaka, The clinical value of frequency analysis of the first heart sound in myocardial infarction, *Circulation*, 41:1003–1014, 1970. ©American Heart Association.



6.2.2 Frequency analysis of murmurs to diagnose valvular defects

Cardiovascular valvular defects and diseases cause high-frequency, noise-like sounds known as murmurs.

Yoshimura et al.: tunable bandpass filter with cutoff

$18 - 1,425 \text{ Hz}$ to process recorded PCG signals.

Diastolic *rumble* of mitral stenosis: $20 - 200 \text{ Hz}$.

Diastolic *blow* of aortic regurgitation: $200 - 1,600 \text{ Hz}$.



van Vollenhoven et al.:

tunable bandpass filter, 50 Hz bandwidth,

center frequency tunable in steps of 50 Hz .

100 ms window in diastolic phase of recorded PCG signals.

Murmur of mitral stenosis: limited to less than 400 Hz .

Aortic insufficiency combined with mitral stenosis:

more high-frequency energy in the range $300 - 1,000 \text{ Hz}$.



Sarkady et al.:

synchronized averaging of PSDs of PCG signals

over several cardiac cycles computed using the FFT.



Johnson et al.:

FFT-based PSDs of systolic murmur (aortic stenosis).

PSDs of systolic windows of duration 86, 170, and 341 *ms*,
averaged over 10 cardiac cycles.

Hypothesis: higher murmur frequencies generated
as the severity of aortic stenosis increases.



Trans-aortic-valvular systolic pressure gradient measured

with catheterization and cardiac fluoroscopy:

$10 - 140 \text{ mm of Hg}$.

Spectral power ratios computed with the bands

$25 - 75 \text{ Hz}$: constant area (CA) related to normal sounds,

$75 - 150 \text{ Hz}$: predictive area (PA) related to murmurs.

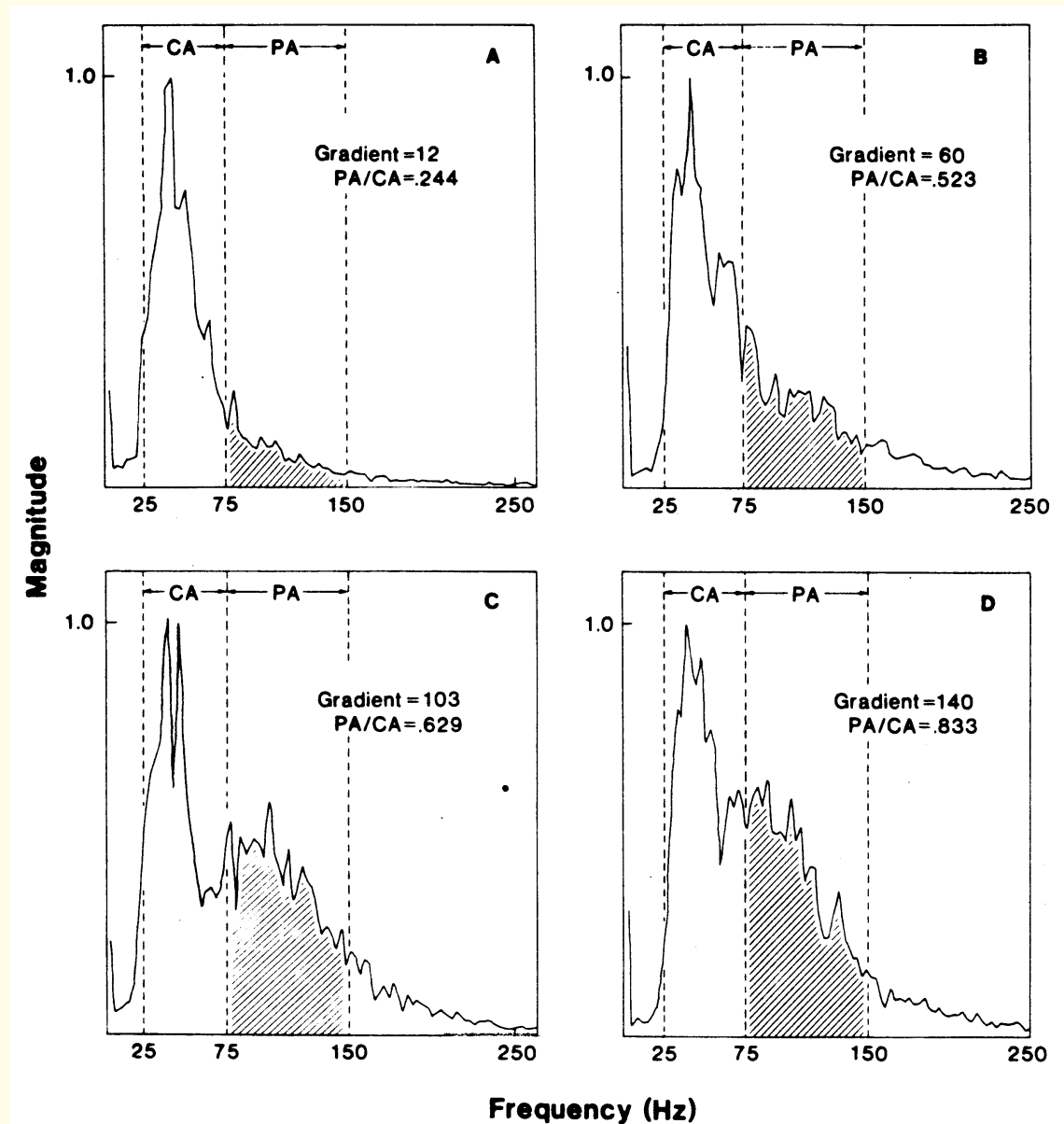


Figure 6.2: Averaged and normalized PSDs of four patients with aortic stenosis of different levels of severity. Each PSD is segmented into two parts: a constant area CA and a predictive area PA . The trans-valvular systolic pressure gradient (measured via catheterization in mm of Hg) and the PA/CA spectral power ratio are shown for each case. Reproduced with permission from the American College of Cardiology: G.R. Johnson, R.J. Adolph, and D.J. Campbell, Estimation of the severity of aortic valve stenosis by frequency analysis of the murmur, *Journal of the American College of Cardiology*, 1(5):1315–1323, 1983 ©Elsevier Science.



6.3 The Fourier Spectrum

Fourier transform: most commonly used transform

to study the frequency-domain characteristics of signals.

Fourier transform uses sinusoidal functions

as its basis functions.



Projections computed of the given signal $x(t)$ onto the complex exponential basis function of frequency ω in *radians/s*:

$$\exp(j\omega t) = \cos(\omega t) + j \sin(\omega t).$$

$$X(\omega) = \int_{-\infty}^{\infty} x(t) \exp(-j\omega t) dt, \quad (6.1)$$



or in the frequency variable f in Hz as

$$X(f) = \int_{-\infty}^{\infty} x(t) \exp(-j2\pi ft) dt. \quad (6.2)$$

This is the *analysis* step of the transform.



Inverse transformation: *synthesis* of the signal $x(t)$ as a

weighted combination of the complex exponential

basis functions:

$$\begin{aligned}x(t) &= \frac{1}{2\pi} \int_{-\infty}^{\infty} X(\omega) \exp(j\omega t) d\omega \\ &= \int_{-\infty}^{\infty} X(f) \exp(j2\pi ft) df.\end{aligned}\quad (6.3)$$



Discrete-time signal $x(n)$, continuous frequency variable ω :

$$X(\omega) = \sum_{n=-\infty}^{\infty} x(n) \exp(-j\omega n). \quad (6.4)$$

Normalized-frequency: $0 \leq \omega \leq 2\pi$ or $0 \leq f \leq 1$.

Lower limit of the summation: 0 if the signal is causal.

Upper limit: index $(N - 1)$ of the last sample

in the case of a finite-duration signal with N samples.



Frequency variable ω may also be defined over $0 \leq \omega \leq \omega_s$,

equivalent to $0 \leq f \leq f_s$;

then n multiplied by the sampling interval T in seconds.

Fourier transform equivalent to z -transform evaluated

on the unit circle with $z = \exp(j\omega)$.

Fourier transform of a sampled signal is periodic:

period = sampling frequency ω_s or

2π (normalized frequency).



When processing digital signals on a computer,

frequency variable ω is sampled, as $\omega = 2\pi \frac{f_s}{N} k$,

or in normalized frequency as $\omega = \frac{2\pi}{N} k$.

k : frequency sample index.

N : number of samples over one period of spectrum $X(\omega)$.



DFT (analysis) relationship:

$$X(k) = \sum_{n=0}^{N-1} x(n) \exp\left(-j \frac{2\pi}{N} k n\right), \quad k = 0, 1, 2, \dots, N-1. \quad (6.5)$$

Assumed that the given signal has N samples.

FT of a discrete-time signal with N samples is

completely determined by N samples of its FT

equally spaced around the unit circle in the z -plane.



Inverse DFT (synthesis) relationship:

$$x(n) = \frac{1}{N} \sum_{k=0}^{N-1} X(k) \exp\left(j \frac{2\pi}{N} k n\right), \quad n = 0, 1, 2, \dots, N-1. \quad (6.6)$$

Sampling the frequency variable causes the signal to become periodic in the time domain.

The equations above define forward and inverse DFTs over one period.



$$\exp\left(j\frac{2\pi}{N}kn\right) = \cos\left(\frac{2\pi}{N}kn\right) + j \sin\left(\frac{2\pi}{N}kn\right) \quad (6.7)$$

Sine and cosine functions of normalized frequency

$$f = \frac{1}{N}k, \quad k = 0, 1, 2, \dots, N - 1.$$

Normalized frequency in the range $0 \leq f \leq 1$;

converted to real frequency in Hz

by multiplication with $f_s Hz$.



DFT Equation 6.5:

dot product or projection of the given signal $x(n)$ onto each complex exponential or sinusoid $\exp(-j\frac{2\pi}{N}kn)$.

Inverse DFT Equation 6.6:

synthesis of the signal $x(n)$ as a linear combination of the complex exponential basis functions, with the weights being the DFT coefficients $X(k)$.



Important properties of the DFT and their implications:

- A signal $x(n)$ and its DFT $X(k)$ are both periodic.
- If a signal $x(n)$ has N samples, its DFT $X(k)$ must be computed with at least N samples equally spaced over the normalized-frequency range $0 \leq \omega \leq 2\pi$ (equivalently, around the unit circle in the z -plane) for complete representation and determination of $X(\omega)$, and exact reconstruction of $x(n) = \text{inverse DFT of } X(k)$.



One may use more than N samples to compute $X(k)$ to employ an FFT algorithm with $L = 2^M \geq N$ samples, or to obtain $X(\omega)$ with finer frequency sampling than $\frac{2\pi}{N}$.

- The DFT is linear:

$$\text{DFT} [a x(n) + b y(n)] = a X(k) + b Y(k).$$

$X(k)$ and $Y(k)$: DFTs of $x(n)$ and $y(n)$.



- DFT $[x(n - n_o)] = \exp(-j \frac{2\pi}{N} k n_o) X(k)$.

A time shift leads to a linear component being added to the phase of the original signal.

All sequences in DFT relationships are periodic: shift operation defined as a circular or periodic shift.

If at least n_o zeros are present or are padded at the end of the signal before the shift operation, a circular shift will be equivalent to a linear shift.



- DFT $[x(n) * h(n)] = X(k) H(k)$.

Inverse DFT $[X(k) H(k)] = x(n) * h(n)$.

Similarly, $x(n) h(n)$ and $X(k) * H(k)$ form a DFT pair.

Convolution in one domain is equivalent to multiplication in the other.

All signals must have the same number of samples N .



All sequences in DFT relationships are periodic:
convolution operations in the DFT relationships are
periodic convolution and not linear convolution.
Circular or periodic convolution defined for
periodic signals having the same period:
result will also be periodic with the same period.



The result of linear convolution of two signals

$x(n)$ and $h(n)$

with different durations N_x and N_h samples, respectively, will have a duration of $N_x + N_h - 1$ samples.

If linear convolution is desired via the

inverse DFT of $[X(k) H(k)]$, the DFTs

must be computed with $L \geq N_x + N_h - 1$ samples.

The signals should be padded with zeros at the end

to make their effective durations equal for

DFT computation and multiplication.

All signals and DFTs are periodic with

the augmented period L .



- DFT of a real signal $x(n)$ possesses conjugate symmetry:
 $X(-k) = X^*(k)$.

Real part and magnitude of $X(k)$: even sequences;
imaginary part and phase of $X(k)$: odd sequences.



- Parseval's theorem: total energy of the signal remains the same before and after Fourier transformation.

$$\int_{-\infty}^{\infty} |x(t)|^2 dt = \frac{1}{2\pi} \int_{-\infty}^{\infty} |X(\omega)|^2 d\omega, \quad (6.8)$$

$$\sum_{n=-\infty}^{\infty} |x(n)|^2 = \frac{1}{2\pi} \int_{-\pi}^{\pi} |X(\omega)|^2 d\omega,$$

$$\sum_{n=0}^{N-1} |x(n)|^2 = \frac{1}{N} \sum_{k=0}^{N-1} |X(k)|^2.$$



Integral of $|X(\omega)|^2$ over all ω or the sum of $|X(k)|^2$ over all k : total energy of the signal, or average power if divided by the duration of the signal. $|X(\omega)|^2$ and $|X(k)|^2$ — power spectral *density* as a function of frequency.



6.4 Estimation of the Power Spectral Density Function

Consider a signal with N samples:

$$x(n), n = 0, 1, 2, \dots, N - 1.$$

To compute the time-averaged ACF

$\phi_{xx}(m)$ for a delay of m samples,

we need to form the product $x(n) x(n \pm m)$

and sum over the available range of data samples.

True ACF: $\phi_{xx}(m) = E[x(n) x(n + m)]$.



We may sum from $n = 0$ to $n = N - 1$ when computing

$\phi_{xx}(0)$ with $x(n) x(n) = x^2(n)$.

However, when computing $\phi_{xx}(1)$ with $x(n) x(n + 1)$,

we can only sum from $n = 0$ to $n = N - 2$.

Linear shift of m samples to compute $\phi_{xx}(\pm m)$:

m samples of one signal drop out of the window of analysis

indicated by the overlap between the

two versions of the signal.



Only $N - |m|$ pairs of data samples available to estimate

ACF for delay of $\pm m$ samples.

Sample-mean estimate of ACF:

$$\phi_1(m) = \frac{1}{N - |m|} \sum_{n=0}^{N-|m|-1} x(n) x(n + m). \quad (6.9)$$



Oppenheim and Schafer:

$\phi_1(m)$ is a consistent estimate of $\phi_{xx}(m)$.

Zero bias and variance that tends to zero as $N \rightarrow \infty$.

Variance of estimate exceptionally large as $m \rightarrow N$:

very few non-zero pairs of samples available

to compute the ACF.



Alternative definition of ACF:

ignore lack of $|m|$ non-zero pairs of samples,

apply same scale factor for all delays:

$$\phi_2(m) = \frac{1}{N} \sum_{n=0}^{N-|m|-1} x(n) x(n+m). \quad (6.10)$$



Upper limit of summation could be $N - 1$:

no effect on the result.

First or last $|m|$ samples of $x(n)$

will not overlap with $x(n + m)$:

result in zero product terms.



Oppenheim and Schafer: $\phi_2(m)$ has bias = $\frac{m}{N} \phi_{xx}(m)$.

Bias tends to actual value being estimated as $m \rightarrow N$.

Variance almost independent of m ,

tends to zero as $N \rightarrow \infty$.

Both ACF estimates asymptotically unbiased;

bias of $\phi_2(m)$ tends to zero as $N \rightarrow \infty$.

Good estimates of ACF if N is large and $m \ll N$.



ACF estimates $\phi_1(m)$ and $\phi_2(m)$ inter-related:

$$\phi_2(m) = \frac{N - |m|}{N} \phi_1(m). \quad (6.11)$$

$\phi_2(m)$ is a scaled version of $\phi_1(m)$.

Scaling factor is a function of m : referred to as a *window*.



6.4.1 The periodogram

PSD and ACF: Fourier transform pair.

$$S_2(\omega) = \sum_{m=-(N-1)}^{N-1} \phi_2(m) \exp(-j\omega m). \quad (6.12)$$

Fourier transform of $x(n)$, $n = 0, 1, 2, \dots, N - 1$:

$$X(\omega) = \sum_{n=0}^{N-1} x(n) \exp(-j\omega n). \quad (6.13)$$



$$S_2(\omega) = \frac{1}{N} |X(\omega)|^2. \quad (6.14)$$

PSD estimate $S_2(\omega)$: *periodogram* of $x(n)$.



Oppenheim and Schaffer:

$S_2(\omega)$ is a biased estimate of the PSD, with

$$E[S_2(\omega)] = \sum_{m=-(N-1)}^{N-1} \frac{N - |m|}{N} \phi_{xx}(m) \exp(-j\omega m). \quad (6.15)$$



Fourier transform of $\phi_1(m)$: a different estimate of PSD.

$$S_1(\omega) = \sum_{m=-(N-1)}^{N-1} \phi_1(m) \exp(-j\omega m). \quad (6.16)$$

$$E[S_1(\omega)] = \sum_{m=-(N-1)}^{N-1} \phi_{xx}(m) \exp(-j\omega m). \quad (6.17)$$

$S_1(\omega)$ is a biased estimate of the PSD.



The two estimates $S_2(\omega)$ and $S_1(\omega)$ may be seen as the

Fourier transforms of windowed ACFs.

Window function for $\phi_2(m)$:

triangular function or Bartlett window.

$$w_B(m) = \begin{cases} \frac{N-|m|}{N}, & |m| < N \\ 0, & \textit{otherwise} \end{cases} . \quad (6.18)$$



Window function for $\phi_1(m)$: rectangular function.

$$w_R(m) = \begin{cases} 1 & |m| < N \\ 0, & \textit{otherwise} \end{cases} . \quad (6.19)$$

The windows have a duration of $(2N - 1)$ samples.



ACF multiplied with window \rightarrow

PSD convolved with FT of window:

leads to spectral leakage and loss of resolution.

Fourier transforms of Bartlett and rectangular windows:

$$W_B(\omega) = \frac{1}{N} \left[\frac{\sin(\omega N/2)}{\sin(\omega/2)} \right]^2, \quad (6.20)$$

$$W_R(\omega) = \frac{\sin[\omega(2N - 1)/2]}{\sin(\omega/2)}. \quad (6.21)$$



Oppenheim and Schafer: periodogram has a

variance that does not approach zero as $N \rightarrow \infty$;

variance of the order of σ_x^4 regardless of N .

The periodogram is not a consistent estimate of the PSD.



6.4.2 *The need for averaging*

Common approach to reduce the variance of an estimate:

average over a number of statistically independent estimates.

A number of periodograms may be computed

over multiple observations of a signal and

averaged to obtain a better estimate of the PSD.



It is necessary for the process to be stationary,
at least over the period over which the
periodograms are computed and averaged.



Problem: *How can we obtain an averaged periodogram*

when we are given only one signal record of finite duration?

Solution: Bartlett method to average

periodograms of segments of the given signal record.



1. Divide given data $x(n)$, $n = 0, 1, 2, \dots, N - 1$, into K segments of M samples each:

$$x_i(n) = x(n + (i-1)M), \quad 0 \leq n \leq M-1, \quad 1 \leq i \leq K. \quad (6.22)$$

2. Compute the periodogram of each segment as

$$S_i(\omega) = \frac{1}{M} \left| \sum_{n=0}^{M-1} x_i(n) \exp(-j\omega n) \right|^2, \quad 1 \leq i \leq K. \quad (6.23)$$

Fourier transform: DFT using the FFT.



3. If ACF $\phi_{xx}(m)$ negligible for $|m| > M$, the periodograms of the K segments with M samples each may be assumed to be mutually independent. Bartlett estimate $S_B(\omega)$ of the PSD = sample mean of the K independent observations of the periodogram:

$$S_B(\omega) = \frac{1}{K} \sum_{i=1}^K S_i(\omega). \quad (6.24)$$



Oppenheim and Schafer: expected value of the

Bartlett estimate $S_B(\omega) =$ convolution of true PSD $S_{xx}(\omega)$

with the FT of Bartlett window.

Bias, spectral smearing, and leakage:

loss of spectral resolution.

Variance tends to zero as number of segments K increases:

consistent estimate of the PSD.



Stationary signal of fixed duration of N samples: limitations

on the number of segments K that we may obtain.

Variance of PSD estimate decreases as K is increased:

but as M decreases, the main lobe of the FT of the

Bartlett window widens; frequency resolution lost.



Cyclo-stationary signals such as the PCG offer a unique and interesting approach to synchronized averaging of periodograms over a number of cycles, without trade-off between reduction of variance and loss of spectral resolution.



6.4.3 *The use of windows: Spectral resolution and leakage*

Bartlett procedure: ensemble averaging approach to reduce the variance of the periodogram.

Another approach: to obtain a smooth spectrum,

convolve periodogram $S(\omega)$ with filter or

smoothing function $W(\omega)$ in the frequency domain

(similar to the use of an MA filter in the time domain).



Smoothed estimate $S_s(\omega)$:

$$S_s(\omega) = \frac{1}{2\pi} \int_{-\pi}^{\pi} S(\nu) W(\omega - \nu) d\nu. \quad (6.25)$$

ν : temporary variable for integration.

PSD: nonnegative function.

Condition on the smoothing function $W(\omega)$:

$$W(\omega) \geq 0, \quad -\pi \leq \omega \leq \pi.$$



Oppenheim and Schafer:

variance of smoothed periodogram reduced by the factor

$$\frac{1}{N} \sum_{m=-(M-1)}^{M-1} w^2(m) = \frac{1}{2\pi N} \int_{-\pi}^{\pi} W^2(\omega) d\omega, \quad (6.26)$$

with reference to variance of original periodogram.

N : total number of samples in signal.

$(2M - 1)$: number of samples in smoothing window.



Rectangular window: variance-reduction factor of $\sim \frac{2M}{N}$.

Bartlett window: variance-reduction factor of $\sim \frac{2M}{3N}$.

Smoothing of spectrum and reduction of variance achieved
at the price of loss of frequency resolution.



Periodogram = FT of ACF estimate $\phi(m)$:

convolution operation in frequency domain in Equation 6.25

equivalent to multiplying $\phi(m)$ with $w(m) = \text{IFT} [W(\omega)]$.

Same PSD estimate as $S_s(\omega)$ obtained by

applying a window to the ACF estimate and

taking the Fourier transform of the result.

ACF is an even function: window should also be even.



Welch's method to average modified periodograms:

Given signal is segmented as in the Bartlett procedure,

but a window is applied to the original signal segments.

Periodograms of windowed segments:

$$S_{W_i}(\omega) = \frac{1}{ME_w} \left| \sum_{n=0}^{M-1} x_i(n) w(n) \exp(-j\omega n) \right|^2, \quad (6.27)$$

$i = 1, 2, \dots, K.$



E_w = average power of window, duration = M samples:

$$E_w = \frac{1}{M} \sum_{n=0}^{M-1} w^2(n). \quad (6.28)$$

Welch PSD estimate $S_W(\omega) =$

average of modified periodograms:

$$S_W(\omega) = \frac{1}{K} \sum_{i=1}^K S_{W_i}(\omega). \quad (6.29)$$



Welch showed that, if the segments are not overlapping, the variance of the averaged modified periodogram is inversely proportional to K , the number of segments used.

Spectral window convolved with the PSD in the frequency domain is proportional to the squared magnitude of the

Fourier transform of the time-domain data window applied:

any type of data window may be used.



Commonly used data windows:

causal, length = N samples, defined for $0 \leq n \leq N - 1$.

Rectangular:

$$w(n) = 1. \quad (6.30)$$

Bartlett (triangular):

$$w(n) = \begin{cases} \frac{2n}{N-1}, & 0 \leq n \leq \frac{N-1}{2}, \\ 2 - \frac{2n}{N-1}, & \frac{N-1}{2} \leq n \leq N - 1. \end{cases} \quad (6.31)$$



Hamming:

$$w(n) = 0.54 - 0.46 \cos\left(\frac{2\pi n}{N-1}\right). \quad (6.32)$$

Hanning (von Hann):

$$w(n) = \frac{1}{2} \left[1 - \cos\left(\frac{2\pi n}{N-1}\right) \right]. \quad (6.33)$$

Blackman:

$$w(n) = 0.42 - 0.5 \cos\left(\frac{2\pi n}{N-1}\right) + 0.08 \cos\left(\frac{4\pi n}{N-1}\right). \quad (6.34)$$

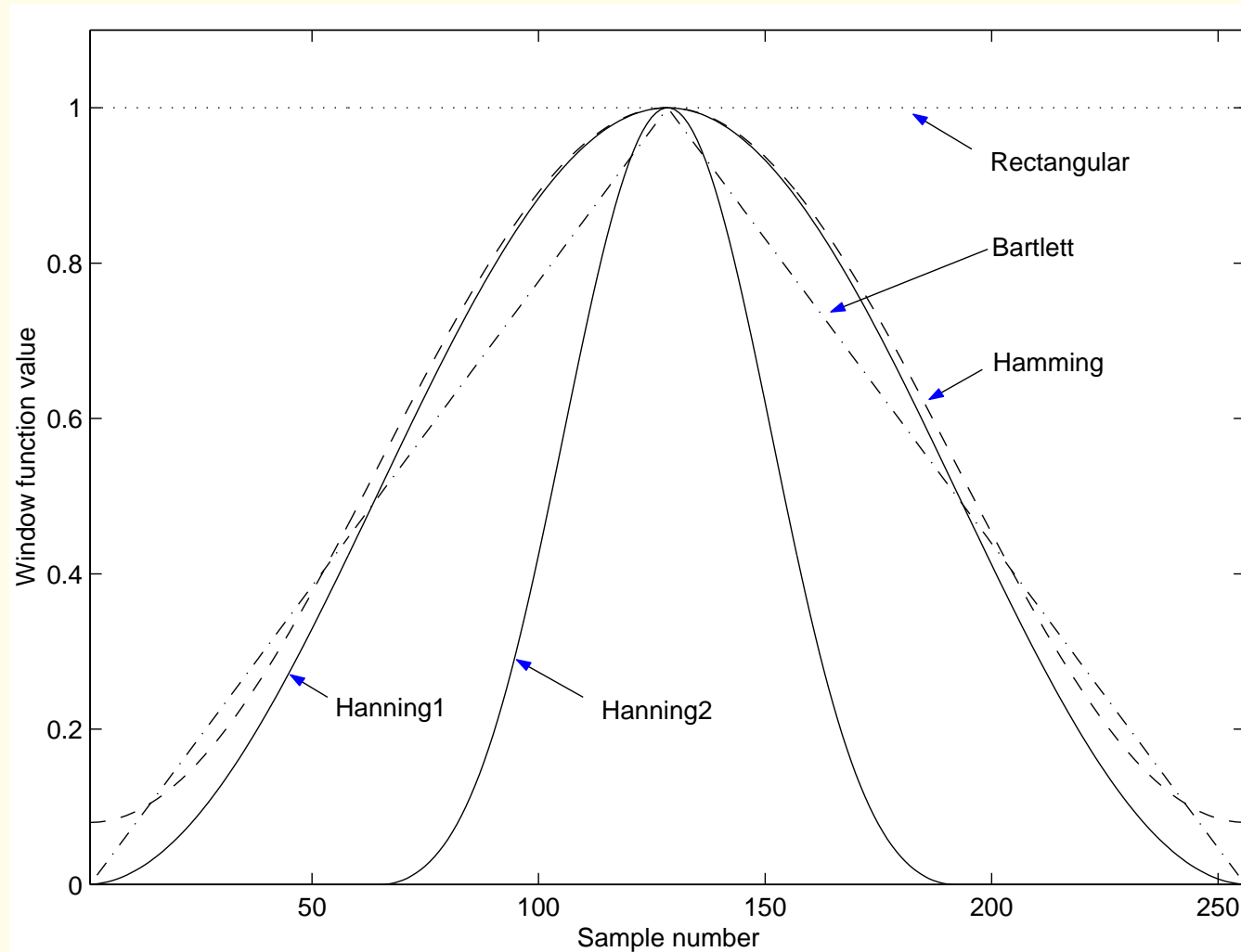


Figure 6.3: Commonly used window functions: rectangular, Bartlett, Hamming, and Hanning windows with $N = 256$ (Hanning1), and Hanning window with $N = 128$ samples (Hanning2). All windows are centered at the 128th sample.



Advantage of tapered windows

(all of the above, except rectangular):

ends of given signal reduced to zero (except Hamming).

No discontinuities in the periodic version of the signal

encountered in DFT-based procedures.

All window functions above are symmetric (even) functions:

linear phase; zero phase if window centered at the origin.

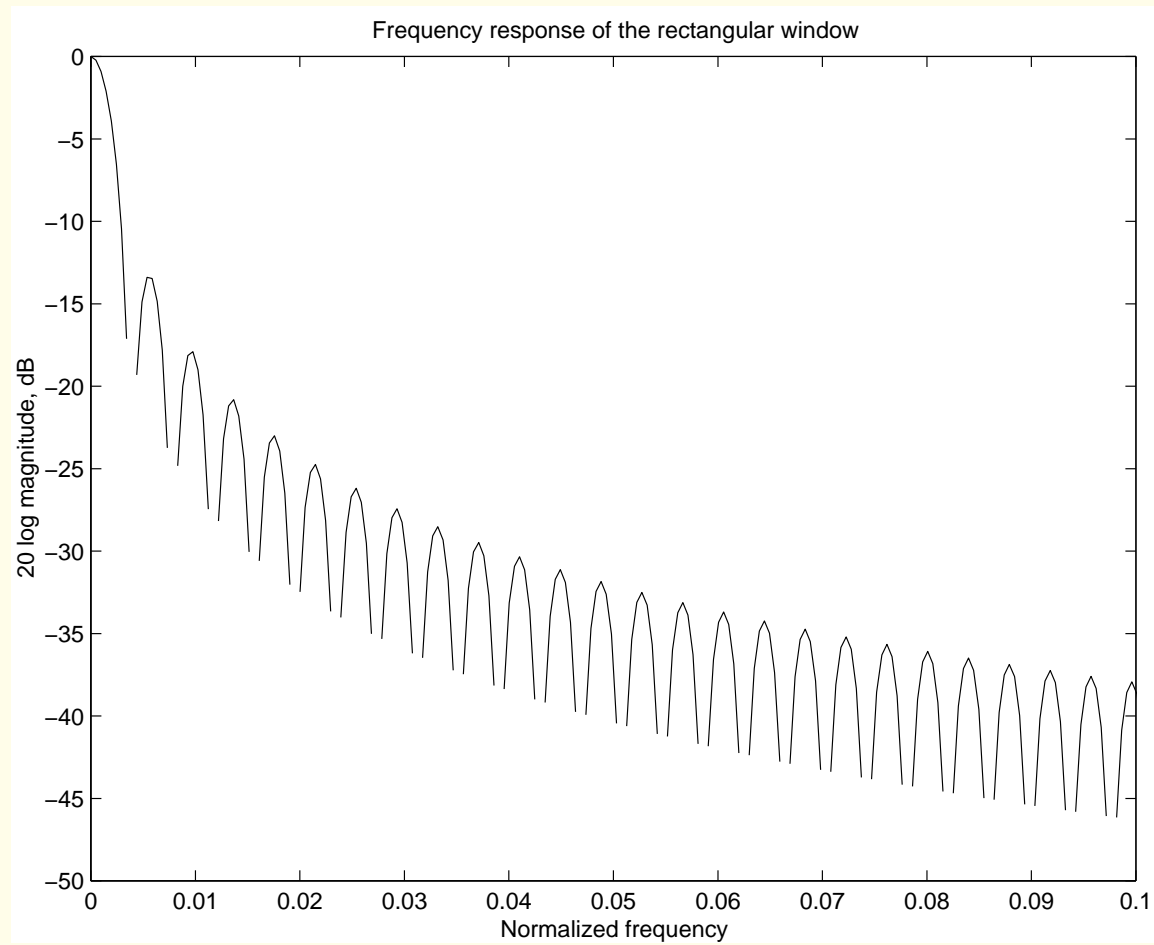


Figure 6.4: Log-magnitude frequency response of the rectangular window illustrated in Figure 6.3. The window width is $N = 256$ samples.

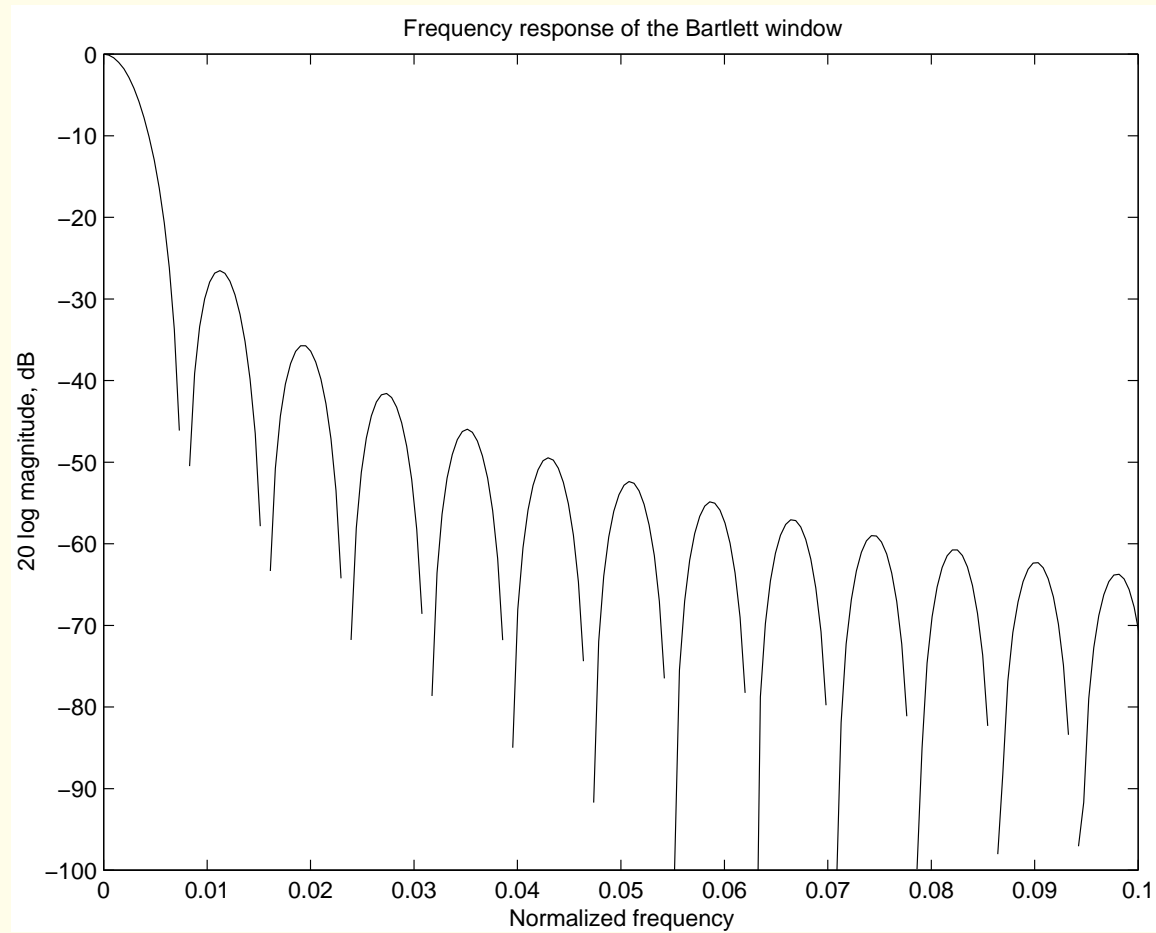


Figure 6.5: Log-magnitude frequency response of the Bartlett window illustrated in Figure 6.3. The window width is $N = 256$ samples.

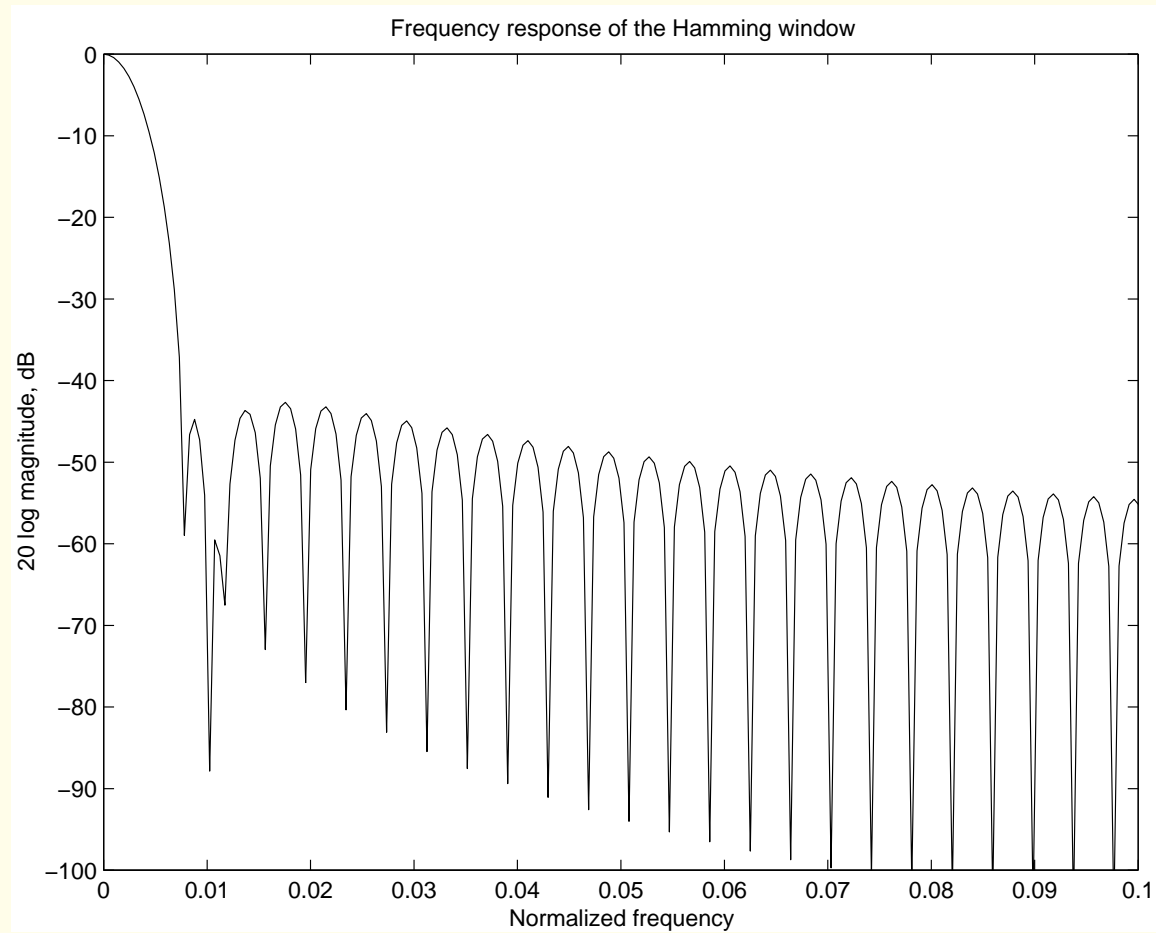


Figure 6.6: Log-magnitude frequency response of the Hamming window illustrated in Figure 6.3. The window width is $N = 256$ samples.

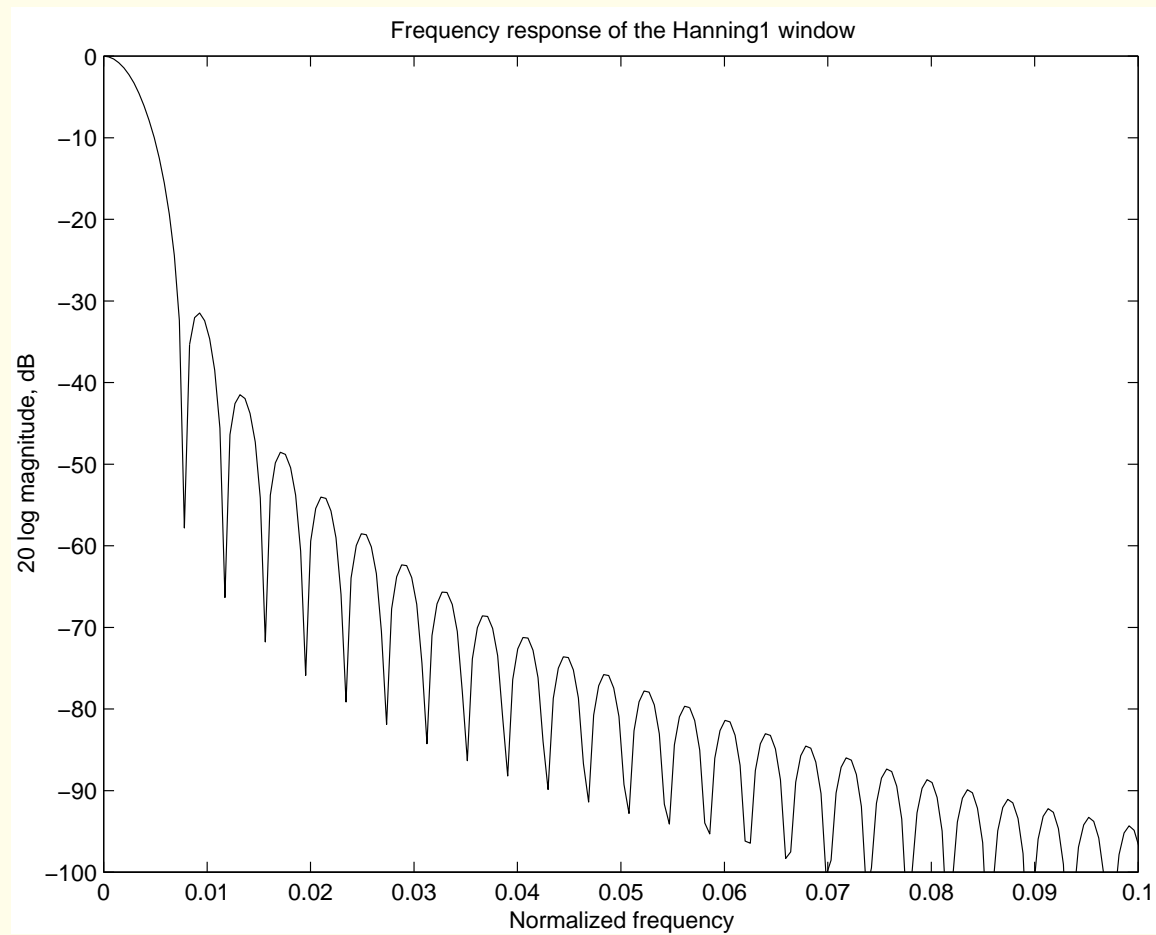


Figure 6.7: Log-magnitude frequency response of the Hanning1 window illustrated in Figure 6.3. The window width is $N = 256$ samples.

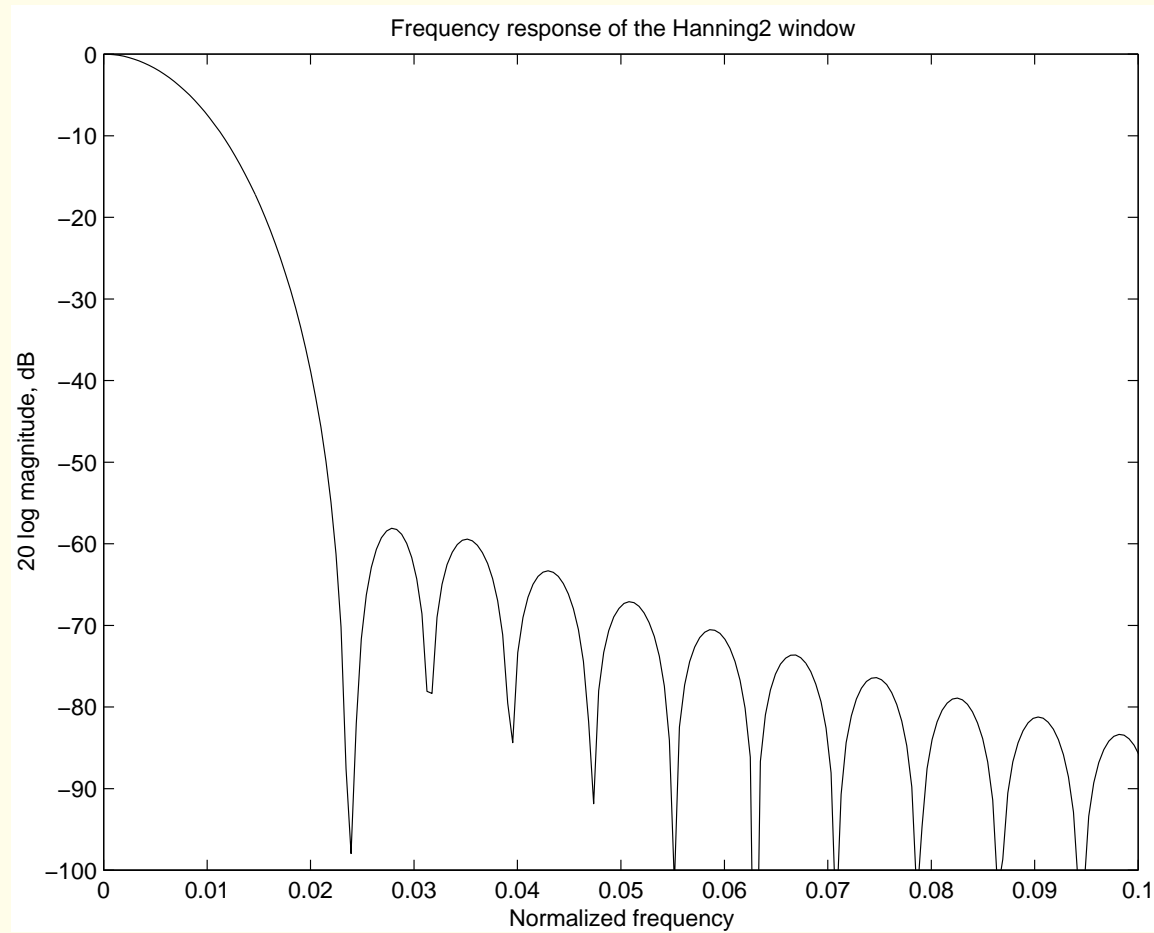


Figure 6.8: Log-magnitude frequency response of the Hanning2 window illustrated in Figure 6.3. The window width is $N = 128$ samples.



Rectangular window: narrowest main lobe of width $\frac{4\pi}{N}$.

Main lobe wider = $\frac{8\pi}{N}$ for Bartlett, Hanning, and Hamming

windows; widest for Blackman window = $\frac{12\pi}{N}$.

Reduction in window width leads to

increase in the main-lobe width.

The wider the main lobe, the greater is the

spectral smoothing: severe loss of spectral resolution.



Rectangular window: highest peak side-lobe = -13 dB .

Bartlett, Hamming, Hanning, and Blackman windows:

peak side-lobe -25 dB , -31 dB , -41 dB , and -57 dB .

Higher side-lobes cause more spectral leakage,

result in a distorted spectrum.

Reduction of leakage with tapered windows comes at the

price of increased main-lobe width: more smoothing and

loss of spectral resolution.

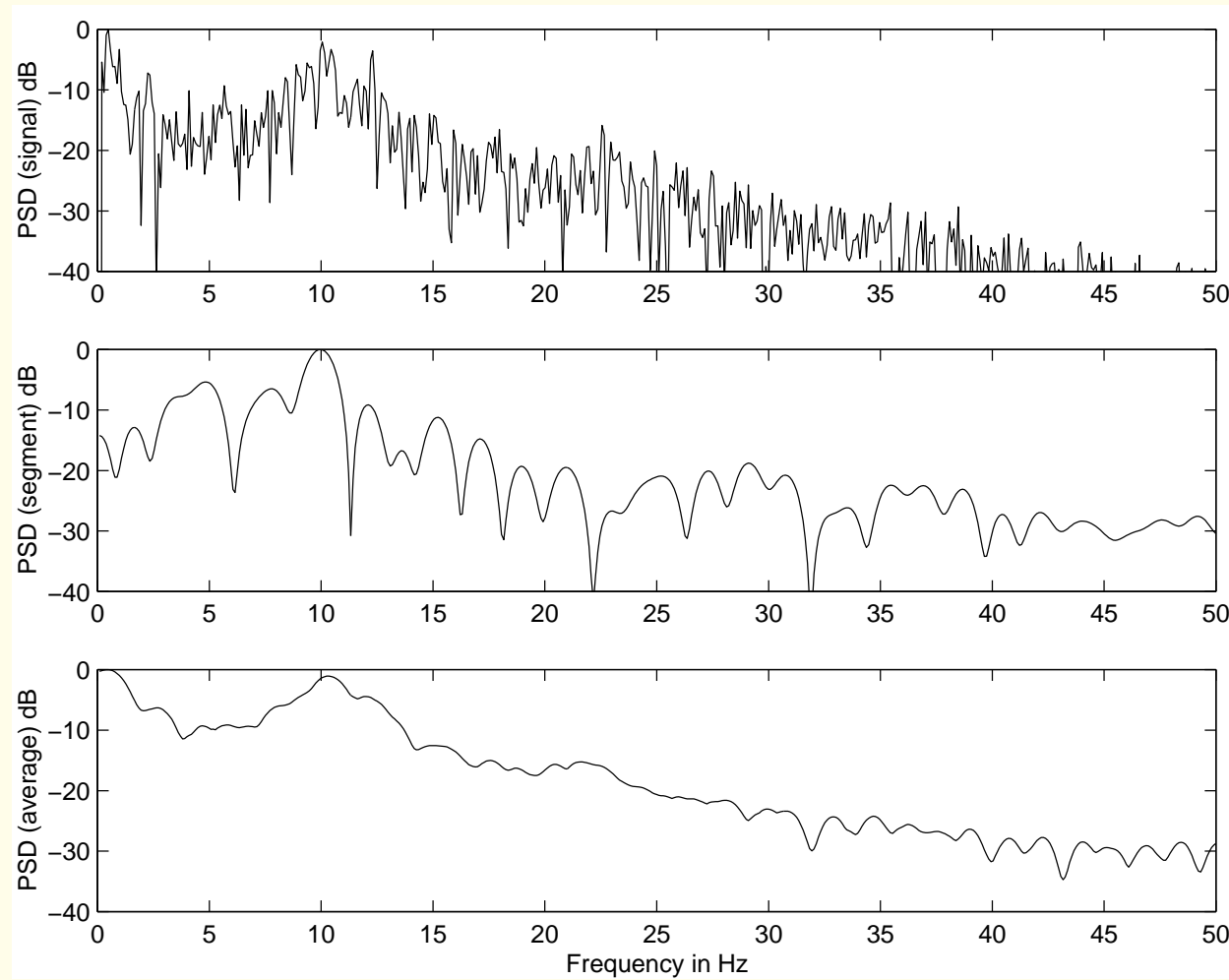


Figure 6.9: Bartlett PSD estimate of the o2 channel of the EEG signal in Figure 1.22. Top trace: PSD of the entire signal. Middle trace: PSD of the 11th segment. Bottom trace: Averaged PSD using $K = 11$ segments of the signal. The rectangular window was (implicitly) used in all cases. Number of samples in the entire signal: $N = 750$. Number of samples in each segment: $M = 64$. All FFT arrays were computed with $L = 1,024$ samples. Sampling frequency $f_s = 100 \text{ Hz}$.

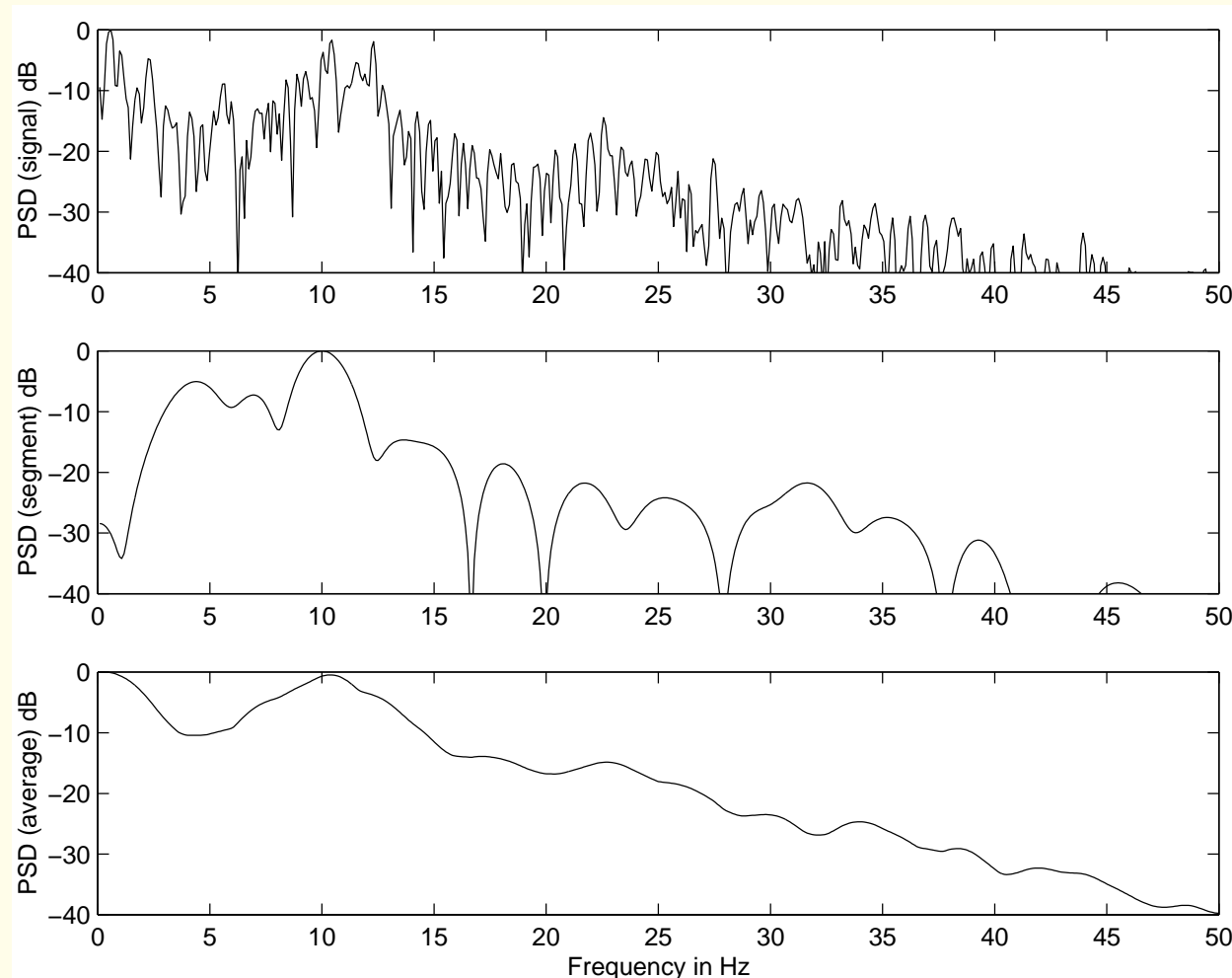


Figure 6.10: Welch PSD estimate of the o2 channel of the EEG signal in Figure 1.22. Top trace: PSD of the entire signal. Middle trace: PSD of the 11th segment. Bottom trace: Averaged PSD using $K = 11$ segments of the signal. The Hanning window was used in all cases. Number of samples in the entire signal and the size of the Hanning window used in computing the PSD of the entire signal: $N = 750$. Number of samples in each segment and the size of the Hanning window used in the averaged periodogram method: $M = 64$. All FFT arrays were computed with $L = 1,024$ samples. Sampling frequency $f_s = 100$ Hz.



Hanning window: smoothing of spurious peaks in PSD.

Wider main-lobe of Hanning window's frequency response:

more severe loss of frequency resolution (smoothing).

Averaged PSD in the lowest trace of Figure 6.10 illustrates

benefit of Hanning window: reduced power for $f > 30 \text{ Hz}$.

Lower side-lobe levels of Hanning window: less leakage

(as compared to the rectangular window).



6.4.4 *Estimation of the autocorrelation function*

Good estimates of ACF required in applications such as design of the optimal Wiener filter and estimation of the statistics of stochastic processes.

After a PSD estimate has been obtained (Bartlett or Welch) take the inverse Fourier transform \rightarrow estimate of ACF.

We may also fit a smooth curve or a parametric model — Gaussian, Laplacian, etc. — to the PSD or ACF.



$$\phi_2(m) = \frac{1}{N} \sum_{n=0}^{N-|m|-1} x(n) x(n+m). \quad (6.35)$$

ACF is an even function: need to compute only for $m > 0$.

ACF estimate = $\frac{1}{N} \times$ linear convolution of $x(n)$ with $x(-n)$.

DFT $[x(n)] = X(k) \rightarrow$ DFT $[x(-n)] = X^*(k)$.

Convolution in time \equiv multiplication in frequency:

obtain $X(k) X^*(k) = |X(k)|^2$, take its inverse DFT.



DFT: circular convolution, not linear convolution.

Pad $x(n)$ with at least $M - 1$ zeros;

M : largest lag for which the ACF is desired.

Compute DFT with at least $L = N + M - 1$ samples;

N : number of samples in the original signal.

Include the above steps in averaged periodogram procedure,

take inverse DFT of final PSD estimate \rightarrow estimate of ACF.

Divide by $\frac{1}{N}$, or divide by $\phi_{xx}(0)$ to get normalized ACF.



6.4.5 Synchronized averaging of PCG spectra

PCG: nonstationary signal.

Amount of blood in each cardiac chamber and

state of contraction of cardiac muscles

change continuously during each cardiac cycle.

S2 usually has more high-frequency content than S1.

PSD of normal PCG changes within about 300 ms .



Valve opening or closing sounds: short duration $\sim 10 \text{ ms}$;

transients with high-frequency character.

Murmurs add another dimension of nonstationarity:

frequency content well beyond that of normal heart sounds.

PSD of abnormal PCG could change within 100 ms .

Individual epochs of S1, S2, valve snaps, and murmurs of

limited durations of $\sim 10 - 300 \text{ ms}$.

Cannot perform segmented averaging (Bartlett or Welch).



The transmission characteristics of the chest wall change during breathing.

PCG at various locations on the chest are subject to different transmission-path effects.

Adult subjects may cooperate in PCG signal acquisition by holding their breath or performing other maneuvers:

no possible with infants and young children in poor health.



Problem: *Propose a method to obtain averaged*

PSD estimates of the systolic and diastolic heart sounds.

Solution: Cyclo-stationarity of PCG — unique approach to average functions of PCG segments corresponding to the same phase of the cardiac cycle cut from multiple beats.

Nonstationarity of the signal within a cardiac cycle:

need to segment phases of PCG cycles.

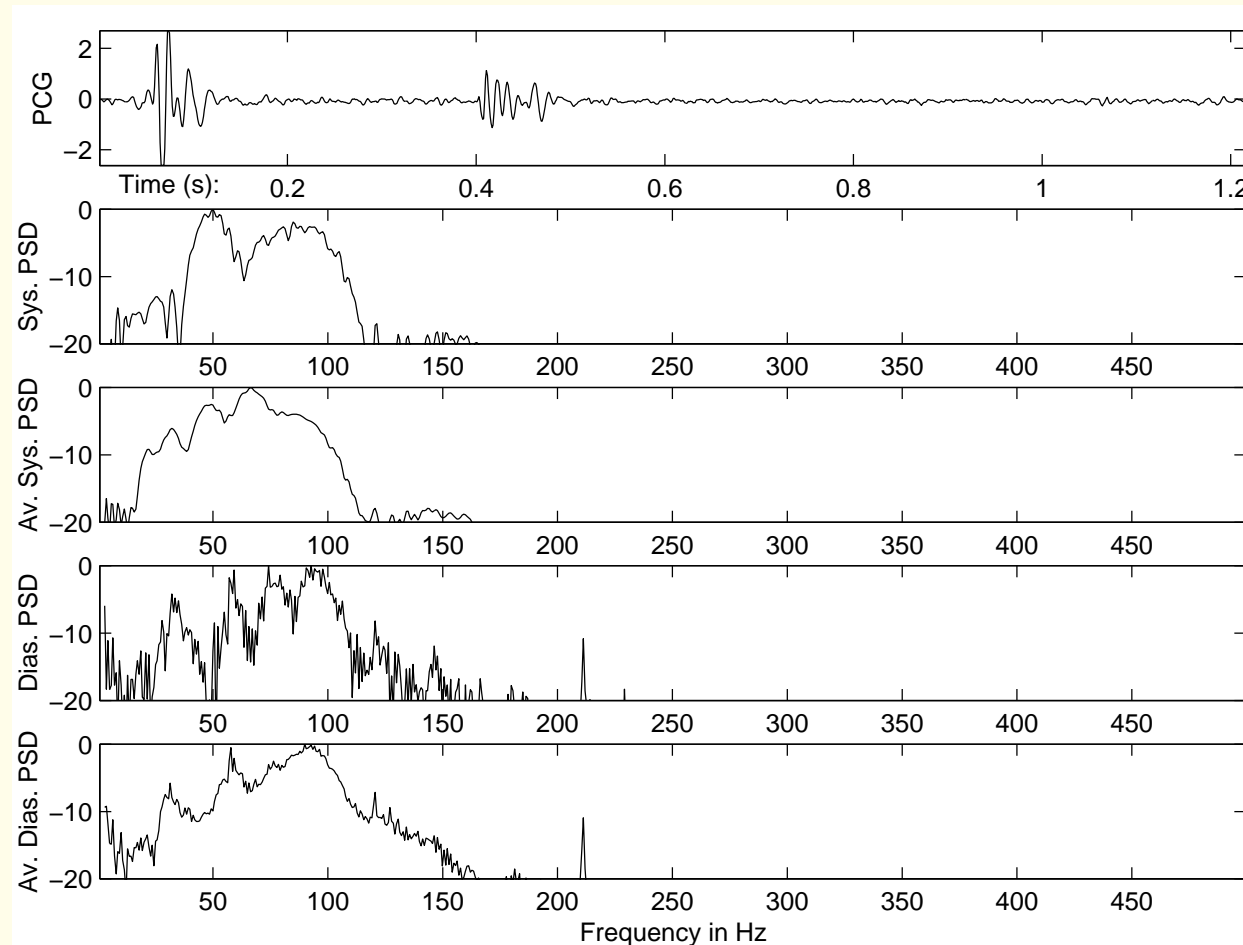


Figure 6.11: Top to bottom: A sample PCG signal over one cardiac cycle of a normal subject (male, 23 years; see also Figures 4.27 and 5.6); periodogram of the systolic portion of the signal (approximately 0 – 0.4 s); averaged periodogram of the systolic parts of 16 cardiac cycles segmented as illustrated in Figure 4.27; periodogram of the diastolic portion of the signal shown in the first plot (approximately 0.4 – 1.2 s); averaged periodogram of the diastolic parts of 16 cardiac cycles. The periodograms are on a log scale (dB).

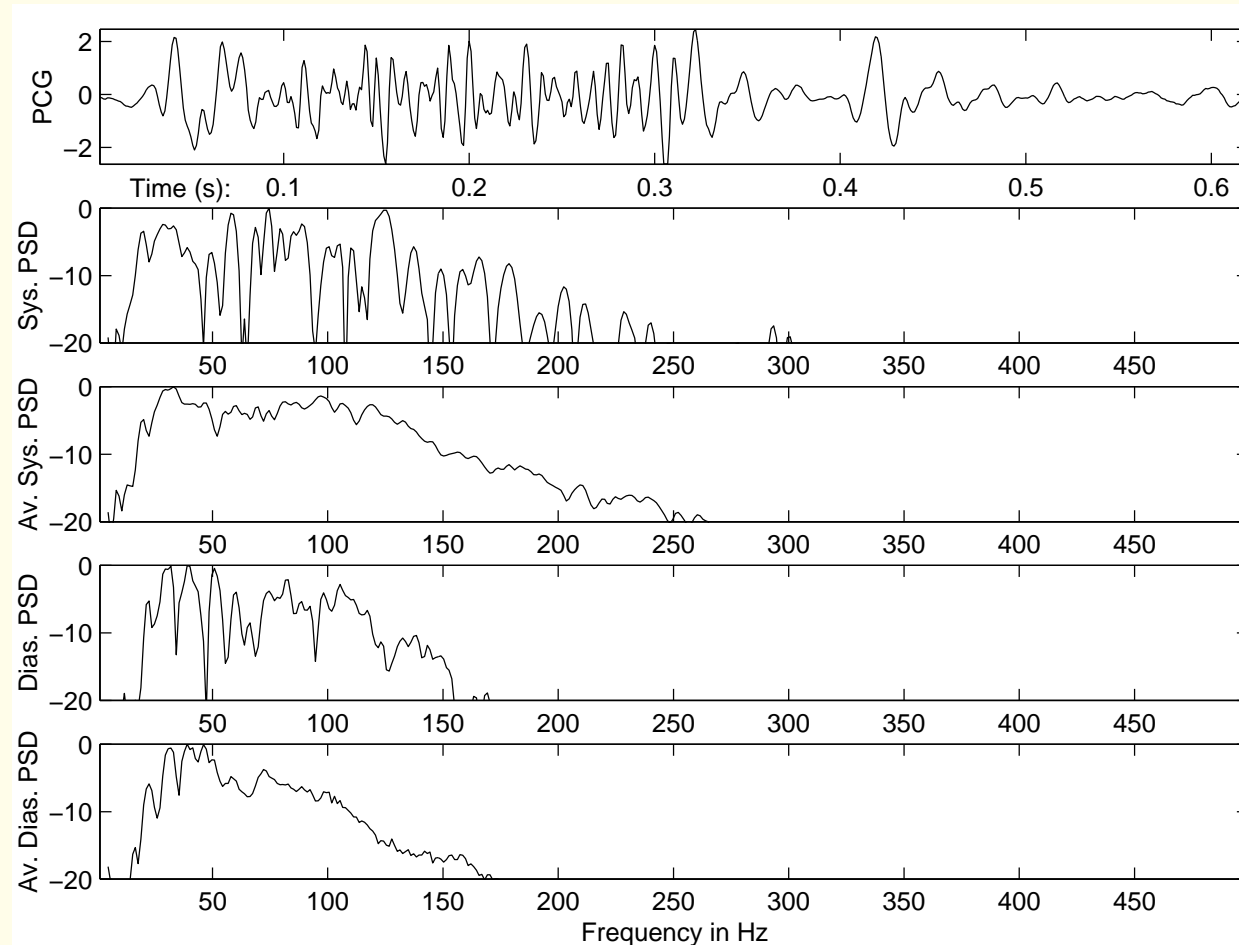


Figure 6.12: Top to bottom: A sample PCG signal over one cardiac cycle of a patient with systolic murmur, split S2, and opening snap of the mitral valve (female, 14 months; see also Figures 4.28 and 5.7); periodogram of the systolic portion of the signal (approximately $0 - 0.28$ s); averaged periodogram of the systolic parts of 26 cardiac cycles segmented as illustrated in Figure 4.28; periodogram of the diastolic portion of the signal shown in the first plot (approximately $0.28 - 0.62$ s); averaged periodogram of the diastolic parts of 26 cardiac cycles. The periodograms are on a log scale (dB).



6.5 Measures Derived from Power Spectral Density Functions

PSD: density function of signal amplitude

or power versus frequency.

Facilitates *nonparametric* and general spectral analysis.

Problem: *Derive parameters or measures from a Fourier*

spectrum or PSD that can help in the characterization

of the spectral variations or features contained therein.



Solution:

PSD is a nonnegative function as well as a density function:

Treat it as a PDF and compute statistics using moments.

Detect peaks corresponding to resonance,

measure their bandwidth or quality factor,

derive measures of concentration of power in

specific frequency bands of interest or concern.



PSD is nonparametric:

but we may derive several parameters that,

while not completely representing the entire PSD,

may facilitate the characterization of

physiological and/or pathological phenomena.



6.5.1 Moments of PSD functions

Area under the PSD = total signal power or energy $\neq 1$.

Normalize all moments by total energy of the signal E_x :

$$\begin{aligned} E_x &= \sum_{n=0}^{N-1} |x(n)|^2 = \frac{1}{N} \sum_{k=0}^{N-1} |X(k)|^2 & (6.36) \\ &= \frac{1}{2\pi} \int_0^{2\pi} |X(\omega)|^2 d\omega = \int_{f_n=0}^1 |X(f_n)|^2 df_n. \end{aligned}$$



Frequency f_n : normalized as $f_n = f/f_s$; $0 \leq f_n \leq 1$.

Replace $|X(\cdot)|^2$ in the above expressions by $S_{xx}(\cdot)$.

In all definitions of moments of PSDs:

$$S_{xx}(k) = \frac{1}{N} |X(k)|^2.$$

$X(k)$: DFT of $x(n)$; $S_{xx}(k)$: PSD of $x(n)$.



Measure of concentration of signal power over its

frequency range: mean frequency $\overline{f} =$ first-order moment

$$\overline{f}_n = \frac{2}{E_x} \int_{f_n=0}^{0.5} f_n S_{xx}(f_n) df_n. \quad (6.37)$$

$$\overline{f}_{Hz} = \frac{f_s}{N} \frac{2}{E_x} \sum_{k=0}^{N/2} k S_{xx}(k). \quad (6.38)$$



Median frequency $f_{med} =$

frequency that splits the PSD in half:

$$f_{med} = \frac{m}{N} f_s \text{ with the largest } m \text{ such that} \quad (6.39)$$

$$\frac{2}{NE_x} \sum_{k=0}^m S_{xx}(k) < \frac{1}{2}; \quad 0 \leq m \leq \frac{N}{2}.$$



Higher-order statistics:

- Variance f_{m2} = second-order moment using $(f_n - \overline{f_n})^2$:

$$f_{m2} = \frac{2}{E_x} \int_{f_n=0}^{0.5} (f_n - \overline{f_n})^2 S_{xx}(f_n) df_n. \quad (6.40)$$

$$f_{m2} = \left(\frac{f_s}{N}\right)^2 \frac{2}{E_x} \sum_{k=0}^{N/2} (k - \overline{k})^2 S_{xx}(k). \quad (6.41)$$

$\overline{k} = N \overline{f_{Hz}} / f_s$ = frequency sample index
corresponding to $\overline{f_{Hz}}$.



- Skewness:

$$\text{skewness} = \frac{f_{m3}}{(f_{m2})^{3/2}}. \quad (6.42)$$

Third-order moment f_{m3} computed with $(f_n - \overline{f_n})^3$:

$$f_{m3} = \frac{2}{E_x} \int_{f_n=0}^{0.5} (f_n - \overline{f_n})^3 S_{xx}(f_n) df_n. \quad (6.43)$$

$$f_{m3} = \left(\frac{f_s}{N}\right)^3 \frac{2}{E_x} \sum_{k=0}^{N/2} (k - \overline{k})^3 S_{xx}(k). \quad (6.44)$$



- Kurtosis:

$$\text{kurtosis} = \frac{f_{m4}}{(f_{m2})^2}. \quad (6.45)$$

Fourth-order moment f_{m4} computed with $(f_n - \overline{f_n})^4$:

$$f_{m4} = \frac{2}{E_x} \int_{f_n=0}^{0.5} (f_n - \overline{f_n})^4 S_{xx}(f_n) df_n. \quad (6.46)$$

$$f_{m4} = \left(\frac{f_s}{N}\right)^4 \frac{2}{E_x} \sum_{k=0}^{N/2} (k - \overline{k})^4 S_{xx}(k). \quad (6.47)$$



Mean frequency: measure of concentration of signal power;

could indicate resonance frequency

of unimodal distributions.

Multiple resonance frequencies: mean frequency not useful.

Multimodal PSDs: series of peak frequencies,

with measures of relative level, bandwidth, or quality factor.



Square-root of f_{m2} : measure of spectral spread.

Skewness = zero if PSD symmetric about mean frequency;

otherwise, indicates extent of asymmetry of distribution.

Kurtosis indicates if PSD is a long-tailed function.



6.5.2 Spectral power ratios

Fraction of signal power in a
frequency band of interest ($f_1 : f_2$)

$$E_{(f_1:f_2)} = \frac{2}{E_x} \int_{f=f_1}^{f_2} |X(f)|^2 df = \frac{2}{NE_x} \sum_{k=k_1}^{k_2} |X(k)|^2. \quad (6.48)$$

k_1 and k_2 : DFT indices corresponding to f_1 and f_2 .

May be computed for several frequency bands.



Johnson et al.: compared integral of magnitude spectrum of
systolic murmurs due to aortic stenosis

over the band $75 : 150 \text{ Hz}$ to that over the band $25 : 75 \text{ Hz}$.

Higher-frequency band: *predictive area* (PA)

of spectrum related to aortic stenosis.

Lower-frequency band: *constant area* (CA)

common to all systolic PCG signal segments.



$$\frac{PA}{CA} = \frac{\int_{f=f_2}^{f_3} |X(f)| df}{\int_{f=f_1}^{f_2} |X(f)| df}. \quad (6.49)$$

$$f_1 = 25 \text{ Hz}, f_2 = 75 \text{ Hz}, f_3 = 150 \text{ Hz}.$$

Figure 6.2:

$\frac{PA}{CA}$ ratio correlates well with severity of aortic stenosis.



Binnie et al.:

spectrum analysis of EEG for detection of epilepsy.

Partitioning or banding of EEG spectrum into not only the

traditional δ , θ , α , and β bands,

but also seven nonuniform bands:

$1 - 2$, $2 - 4$, $4 - 6$, $6 - 8$, $8 - 11$, $11 - 14$, and > 14 Hz .

Additional features related to form factor used.



Study with 275 patients with suspected epilepsy:

90% of signals of patients with epilepsy

classified as abnormal;

86% of patients with EEGs classified as abnormal

had epilepsy.



6.6 Application: Evaluation of Prosthetic Heart Valves

Efficient opening and closing actions of cardiac valves of paramount importance for proper pumping of blood by the heart.

When native valves fail, they may be replaced by mechanical prosthetic valves or by bioprosthetic valves.



Mechanical prosthetic valves prone to sudden failure

due to fracture of their components.

Bioprosthetic valves fail gradually due to tissue

degeneration and calcification: last for 7 – 12 years.

Follow-up of the health of patients with prosthetic valves

requires periodic, noninvasive assessment of the

functional integrity of the valves.



Problem: *Deposition of calcium causes the normally pliant and elastic bioprosthetic valve leaflets to become stiff.*

Propose a method to assess the functional integrity of bioprosthetic valves.



Solution: Increased stiffness of a valve expected to lead to higher-frequency components in its opening or closing sounds.

Durand et al. studied spectra of S1 to evaluate sounds contributed by closure of porcine (pig) bioprosthetic valves implanted in the mitral position in humans.



Normal S1 spectra: limited in bandwidth to about 100 Hz .

Degenerated bioprosthetic valves: significant spectral

energy in the range $100 - 250\text{ Hz}$.



Spectral parameters used by Durand et al.:

first and second dominant peak frequencies;

median frequency;

bandwidth and quality factor of dominant peak;

integrated mean area above -20 *dB*;

highest frequency at -3 *dB*;



total area and *RMS* value of spectrum;

area and *RMS* value in the bands

20 – 100, 100 – 200, 200 – 300 *Hz*.

Normal versus degenerated valve classification

accuracy: 98%.

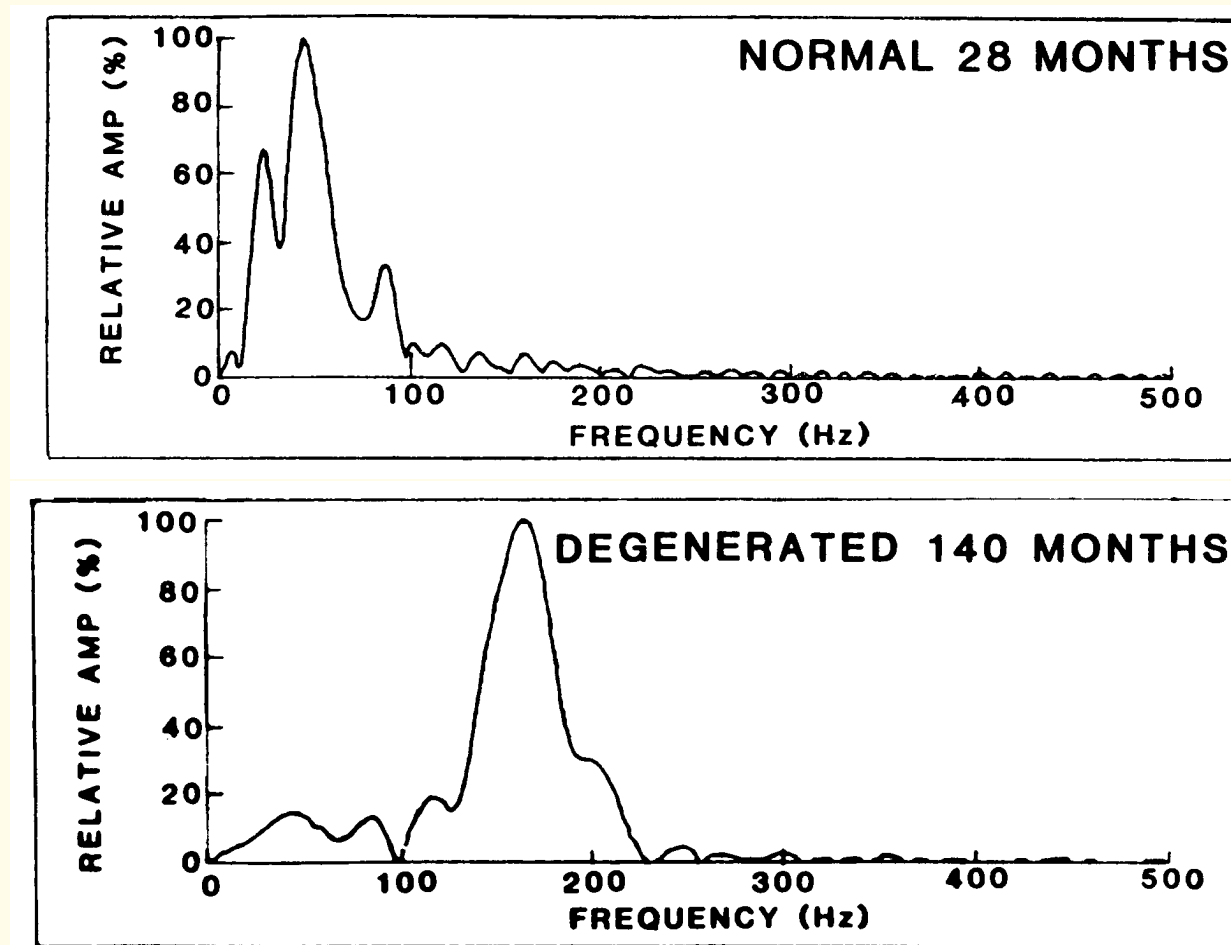


Figure 6.13: First heart sound spectra in the case of normal and degenerated porcine bioprosthesis valves implanted in the mitral position. Reproduced with permission from L.G. Durand, M. Blanchard, G. Cloutier, H.N. Sabbah, and P.D. Stein, Comparison of pattern recognition methods for computer-assisted classification of spectra of heart sounds in patients with a porcine bioprosthesis valve implanted in the mitral position, *IEEE Transactions on Biomedical Engineering*, 37(12):1121–1129, 1990 ©IEEE.